university of groningen

University Medical Center Groningen

University of Groningen

A phase field method for joint denoising, edge detection, and motion estimation in image sequence processing

Preusser, T.; Droske, M.; Garbe, C. S.; Telea, A.; Rumpf, M.

Published in:
Siam Journal on Applied Mathematics

DOI:
10.1137/060677409

IMPORTANT NOTE: You are advised to consult the publisher's version (publisher's PDF) if you wish to cite from it. Please check the document version below.

Document Version
Publisher's PDF, also known as Version of record

Publication date:
2007

Link to publication in University of Groningen/UMCG research database

Citation for published version (APA):
Preusser, T., Droske, M., Garbe, C. S., Telea, A., & Rumpf, M. (2007). A phase field method for joint denoising, edge detection, and motion estimation in image sequence processing. *Siam Journal on Applied Mathematics*, *68*(3), 599-618. https://doi.org/10.1137/060677409

Copyright
Other than for strictly personal use, it is not permitted to download or to forward/distribute the text or part of it without the consent of the author(s) and/or copyright holder(s), unless the work is under an open content license (like Creative Commons).

The publication may also be distributed here under the terms of Article 25fa of the Dutch Copyright Act, indicated by the “Taverne” license. More information can be found on the University of Groningen website: https://www.rug.nl/library/open-access/self-archiving-pure/taverne-amendment.

Take-down policy
If you believe that this document breaches copyright please contact us providing details, and we will remove access to the work immediately and investigate your claim.

Downloaded from the University of Groningen/UMCG research database (Pure): http://www.rug.nl/research/portal. For technical reasons the number of authors shown on this cover page is limited to 10 maximum.

SIAM J. APPL. MATH.
Vol. 68, No. 3, pp. 599–618
© 2007 Society for Industrial and Applied Mathematics

A PHASE FIELD METHOD FOR JOINT DENOISING, EDGE DETECTION, AND MOTION ESTIMATION IN IMAGE SEQUENCE PROCESSING*

T. PREUSSER†, M. DROSKE‡, C. S. GARBE§, A. TELEA¶, AND M. RUMPF‡

Abstract. The estimation of optical flow fields from image sequences is incorporated in a Mumford–Shah approach for image denoising and edge detection. Possibly noisy image sequences are considered as input and a piecewise smooth image intensity, a piecewise smooth motion field, and a joint discontinuity set are obtained as minimizers of the functional. The method simultaneously detects image edges and motion field discontinuities in a rigorous and robust way. It is able to handle information on motion that is concentrated on edges. Inherent to it is a natural multiscale approximation that is closely related to the phase field approximation for edge detection by Ambrosio and Tortorelli. We present an implementation for two-dimensional image sequences with finite elements in space and time. This leads to three linear systems of equations, which have to be solved in a suitable iterative minimization procedure. Numerical results and different applications underline the robustness of the approach presented.

Key words. image processing, phase field method, Mumford–Shah, optical flow, denoising, edge detection, segmentation, finite element method

AMS subject classifications. 62H20, 62H35, 65U10, 65N30

DOI. 10.1137/060677409

1. Introduction.

The task of motion estimation from image sequences, or computing the visual representation as optical flow, is a fundamental problem in computer vision. For a number of applications, a dense motion or optical flow field is desirable, yielding a representation of the motion of observed objects for each pixel of the image sequence. In low-level image processing, the accurate computation of object motion in scenes is a long-standing problem which has been addressed extensively. In particular, global variational approaches initiated by the work of Horn and Schunck [19] are increasingly popular. Initial problems such as the smoothing of discontinuities or high computational cost have been solved successfully [25, 7, 8]. Motion estimation also yields important indicators for the detection and recognition of the observed objects. While a number of techniques first estimate the optical flow field and segment objects later in a second phase [37], an approach of computing motion as well as segmenting objects at the same time is much more appealing. First advances in this direction were investigated in [33, 27, 28, 9, 23, 30]. In particular, Kornprobst et al. [22, 3, 4] have considered piecewise smooth motion patterns on image sequences characterized by piecewise smooth objects. Their results are phrased rigorously on the space of

*Received by the editors December 11, 2006; accepted for publication (in revised form) August 24, 2007; published electronically December 7, 2007. This work has been funded by the Priority Program 1114 "Mathematical methods for time series analysis and digital image processing" of the German Research Foundation (DFG).
http://www.siam.org/journals/siap/68-3/67740.html

†Center of Complex Systems and Visualization (CeVis), University of Bremen, Germany (tp@mevis.de).

‡Institute for Numerical Simulation (INS), University of Bonn, Germany (droske@ins.uni-bonn.de, martin.rumpf@ins.uni-bonn.de).

§Interdisciplinary Center for Scientific Computing (IWR), University of Heidelberg, Germany (Christoph.Garbe@iwr.uni-heidelberg.de).

¶Institute for Mathematics and Computer Science, University of Groningen, The Netherlands (a.c.telea@rug.nl).

Copyright © by SIAM. Unauthorized reproduction of this article is prohibited.

functions of bounded variation (BV), and they propose suitable approximations for the numerical implementation. Already, in [22] a joint approach for the segmentation of moving objects in front of a still background and the computation of motion velocities has been proposed. For a given intensity function on an image sequence, a total variation (TV) type functional for the motion field—which allows for jumps in the optical flow velocity—is analyzed in [4, 3]. Recently, Papenberg et al. [29] considered another TV regularization of the motion field and optical flow constraints involving higher order gradients.

The idea of combining different image processing tasks into a single model in order to cope with interdependencies has drawn attention in several different fields. In image registration, for instance, a joint discontinuity approach for simultaneous registration, segmentation, and image restoration has been proposed by Droske and Ring [15] and extended in [16] to incorporate phase field approximations. In these approaches, the phase field is used to describe object boundaries, and sharp interfaces of zero width are replaced by diffuse interfaces of finite width ϵ in which the phase field variable continuously changes its value from 0 to 1. This description of object boundaries draws its name from physics, where it is used for modeling solidification of fluids and associated phase boundaries [31, 38]. Kapur, Yezzi, and Zöllei [20] and Unal et al. [35] have combined segmentation and registration by applying geodesic active contours described by level sets in both images. Vemuri et al. have also used a level set technique to exploit a reference segmentation in an atlas [36]. We refer to [14] for further references.

Recently, Keeling and Ring [21] investigated the relation between optimization and optical flow extraction. A first approach which relates optical flow estimation to Mumford–Shah image segmentation was presented by Nesi [26]. Recently, Rathi et al. investigated active contours for joint segmentation and optical flow extraction [32]. Cremers and Soatto [13, 12] presented an approach for joint motion estimation and motion segmentation with one functional. Incorporating results from Bayesian inference, they derived an energy functional, which can be seen as an extension of the well-known Mumford–Shah [24] approach. Their functional involves the length of boundaries separating regions of different motion as well as a "fidelity term" for the optical flow assumption. Brox, Bruhn, and Weickert [7] present a Chan–Vese-type model for piecewise smooth motion extraction. For given fixed image data the decomposition of image sequences into regions of homogeneous motion is encoded in a set of level set functions, and the regularity of the motion fields in these distinct regions is controlled by a TV functional. Our approach is in particular inspired by these investigations.

We combine denoising and edge detection with the estimation of motion. This results in an energy functional, which incorporates fidelity and smoothness terms for both the image sequence and the flow field. Our focus lies in particular on motion information that is concentrated on edges such as in the case of a moving object with sharp edge contours but without shading and texture. To cope with this, we formulate the optical flow equations appropriately in regions away from edges and on the edge set. Moreover, we incorporate an anisotropic enhancement of the flow along the edges of the image in the sense of Nagel and Enkelmann [25]. This effectively allows us to spread motion information from the edge set onto the whole domain of a moving object. The model is implemented using the phase field approximation in the spirit of Ambrosio and Tortorelli's approach [2] for the original Mumford–Shah functional. The identification of edges is phrased in terms of a phase field function; no a priori knowledge of objects is required, as opposed to formulations of

Copyright © by SIAM. Unauthorized reproduction of this article is prohibited.

explicit contours. *Particular focus is on optical flow constraints which are not only continuously distributed over shaded or textured regions, but also might be concentrated on edges, e.g., in case of moving objects without texture and shading.* In contrast to a level set approach, the built-in multiscale of the phase field model enables a natural cascadic energy relaxation approach and thus an efficient computation. Indeed, no initial guess for the edge set and the motion field will be required. We present here a truly $(d+1)$-dimensional algorithm, considering time as an additional dimension to the d-dimensional image data. This fully demonstrates the conceptual advantages of the joint approach. Nevertheless, a transfer of the method for only two consecutive time frames is possible but not investigated here. The characteristics of our approach are as follows:

- The distinction of smooth motion fields and optical flow discontinuities is directly linked to edge detection, improving the reliability of the motion estimation.
- The denoising and segmentation task will profit from the explicit coupling of the sequence via the assumption of brightness constancy.
- The phase field approximation is expected to converge to a limit problem for vanishing scale parameter, with a strict notion of edges and motion field discontinuities not involving any additional filtering parameter.
- The algorithm is based on an iteration. In each step a set of three relatively simple linear systems have to be solved for the image intensity, the edge description via the phase field, and the motion field, respectively. Only a small number of iterations is required.

This paper is organized as follows: In section 2 Mumford–Shah-type image denoising and edge detection are reviewed, in section 3 we discuss a generalized optical flow equation, and in section 4 the minimization problem is presented. Section 5 shows how to approximate the segmentation in terms of a variational phase field model. Furthermore, we prove existence of solutions of this model and discuss the limit behavior. Section 6 propounds the corresponding Euler–Lagrange equations, which are discretized applying the usual finite element method in section 7. We conclude with the results in section 8. Finally, in the appendix we provide explicit formulas of all matrices and vectors appearing in the implementation to enable readers to reproduce the algorithm.

2. Recalling the Mumford–Shah functional. In their pioneering paper, Mumford and Shah [24] proposed the minimization of the following energy functional:

$$E_{MS}[u,S] = \lambda \int_\Omega (u-u_0)^2 \,\mathrm{d}\mathcal{L} + \frac{\mu}{2} \int_{\Omega\setminus S} |\nabla u|^2 \,\mathrm{d}\mathcal{L} + \nu \mathcal{H}^{d-1}(S), \tag{2.1}$$

where u_0 is the initial image defined on an image domain $\Omega \subset \mathbb{R}^d$ and λ, μ, ν are positive weights. Here, one asks for a piecewise smooth representation u of u_0 and an edge set S, such that u approximates u_0 in the least squares sense, u ought to be smooth apart from the free discontinuity set S, and in addition S should be smooth and thus small with respect to the $(d-1)$-dimensional Hausdorff measure $\mathcal{H}^{d-1}$. Mathematically, this problem has been treated in the space of functions of bounded variation BV, more precisely in the specific subset SBV [1]. In this paper, we will pick up a phase field approximation for the Mumford–Shah functional (2.1) proposed by Ambrosio and Tortorelli [2]. They describe the edge set S by a phase field ζ which is supposed to be small on S and close to 1 apart from edges, i.e., one asks for

Copyright © by SIAM. Unauthorized reproduction of this article is prohibited.

minimizers of the energy functional

$$E_\epsilon[u,\zeta] = \int_\Omega \lambda(u-u_0)^2 + \frac{\mu}{2}(\zeta^2+k_\epsilon)\,|\nabla u|^2 + \nu\epsilon\,|\nabla\zeta|^2 + \frac{\nu}{4\epsilon}(1-\zeta)^2\,\mathrm{d}\mathcal{L}, \tag{2.2}$$

where ϵ is a scale parameter and $k_\epsilon = o(\epsilon) \ll 1$ a small positive regularizing parameter, which mathematically ensures strict coercivity with respect to u. On edges the weight ζ^2 is expected to vanish. Hence, the second term measures smoothness of u but only away from edges. The last two terms in the integral encode the approximation of the $(d-1)$-dimensional area of the edge set and the strong preference for a phase field value $\zeta \approx 1$ far from edges, respectively. For larger ϵ one obtains coarse, blurred representations of the edge sets and corresponding smoother images u. With decreasing ϵ we successively refine the representation of the edges and include more image details.

3. Generalized optical flow equation. In image sequences we observe different types of motion fields: locally smooth motion visible via variations of object shading and texture in time, or jumps in the motion velocity apparent at edges of objects moving in front of a background. We aim for an identification of corresponding piecewise smooth optical flow fields in piecewise smooth image sequences

$$u : [0,T]\times\Omega \mapsto \mathbb{R}; \quad (t,x) \to u(t,x)$$

for a finite time interval $[0,T]$ and a spatial domain $\Omega \subset \mathbb{R}^d$ with $d = 1,2,3$. In what follows, we assume $\partial\Omega$ to be Lipschitz. The flow fields are allowed to jump on edges in the image sequence. On edges, the derivative Du splits into a singular and a regular part. The regular part is a classical gradient $\nabla_{(t,x)}u$ in space and time, whereas the singular part lives on the singularity set S—the set of edge surfaces in space-time. Time slices of S are the actual image edges at the specific time. We denote by $n_S \in \mathbb{R}^{d+1}$ the normal on S with respect to space-time. The singular part represents the jump of the image intensity on S, i.e., one observes that $D^s u = (u^+ - u^-)n_S$. Here, u^+ and u^- are the upper and lower intensity values on both sides of S, respectively. Now, we suppose that the image sequence u reflects an underlying motion with a piecewise smooth motion velocity v, which is allowed to jump only on S. Thus, S represents object boundaries moving in front of a background, which might as well be in motion. In strict mathematical terms, we suppose that $u, v \in SBV$ (the set of functions of bounded variation and vanishing Cantor part in the gradient) [17, 1]. In this general setting without any smoothness assumption on u and v, we have to ask for a generalized optical flow equation. In fact, away from moving object edges we derive, as usual, from the brightness constancy constraint equation (BCCE) $u(t+s,\, x+s\,v) = \text{const}$ on motion trajectories $\{(t+s,\, x+s\,v) \mid s \in [0,T]\}$, that

$$\nabla_{(t,x)}u \cdot w = 0, \tag{3.1}$$

where $w = (1,v)$ is the space-time motion velocity. On edges, the situation is more complex and in general requires prior knowledge. For instance, a white circular disk moving in front of a black background is visually identical to a black mask with a circular hole moving with the same speed on a white background (the aperture problem). Hence, it is ambiguous on which side of the edge $w^\pm$ vanishes and on which side a nontrivial optical flow equation $n_S \cdot w^\pm = 0$ holds. We will not resolve this ambiguity via semantic assumptions. In what follows, we assume instead that locally only one object—in our example either the circle or the mask—is moving on

Copyright © by SIAM. Unauthorized reproduction of this article is prohibited.

a stationary background. Hence, we rule out that foreground and background are in motion. In other words, our background is that part of the image which is not moving. Then one of the two values of w on both sides of the edge vanishes by assumption, and we can rewrite the optical flow constraint on the edge without identifying foreground or background by

$$n_S \cdot (w^+ + w^-) = 0. \tag{3.2}$$

This in particular includes the case of a sliding motion without any modification of the object overlap, where $n_S \cdot w^+ = n_S \cdot w^- = 0$.

4. Mumford–Shah approach to optical flow. Now, we ask for a simultaneous denoising, segmentation, and flow extraction on image sequences. Hence, we will incorporate the motion field generating an image sequence into a variational method. Let us formulate a corresponding minimization problem in the spirit of the Mumford–Shah model.

DEFINITION 4.1 (Mumford–Shah-type optical flow approach). *Given a noisy initial image sequence $u_0 : D \to \mathbb{R}$ on the space-time domain $D = [0,T] \times \Omega$, we define the energy*

$$\begin{aligned} E_{\mathrm{MSopt}}[u,w,S] = &\int_D \frac{\lambda_u}{2}(u-u_0)^2 \,\mathrm{d}\mathcal{L} + \int_{D\setminus S} \frac{\lambda_w}{2}\left(w \cdot \nabla_{(t,x)} u\right)^2 \mathrm{d}\mathcal{L} \\ &+ \int_{D\setminus S} \frac{\mu_u}{2}\left|\nabla_{(t,x)} u\right|^2 \mathrm{d}\mathcal{L} + \int_{D\setminus S} \frac{\mu_w}{q}\left|\nabla_{(t,x)} w\right|^q \mathrm{d}L + \nu \mathcal{H}^d(S) \end{aligned} \tag{4.1}$$

for a piecewise smooth image sequence u, and a piecewise smooth motion field $w = (1,v)$ with a joint jump set S. Furthermore, we require the optical flow constraint $n_S \cdot (w^+ + w^-) = 0$ on S from (3.2). Now, one asks for a minimizer (u,w,S) of the corresponding constraint minimization problem.

The first and second terms of the energy are fidelity terms with respect to the image intensity and the regular part of the optical flow constraint, respectively. The third and fourth terms encode the smoothness requirement of u and w. Finally, the last term represents the area of the edge surfaces S. The fidelity weights λ_u, λ_w, the regularity weights μ_u, μ_w, and the weight ν controlling the phase field are supposed to be positive and $q \geq 2$. Let us emphasize that, without any guidance from the local time modulation of shading or texture on both sides of an edge, there is still an undecidable ambiguity with respect to foreground and background.

5. Phase field approximation. Similar to the original model for denoising and edge detection (2.1), the above Mumford–Shah approach (4.1) with its explicit dependence on the geometry of the edge set is difficult to implement without any additional strong assumptions either on the image sequence or on the motion field. For a corresponding parametric approach we refer to the recent results by Cremers and Soatto [13, 12]. The level set approach recently presented by Brox, Bruhn, and Weickert [7] does not explicitly encode motion concentrated on edges. We do not aim to impose any additional assumption on the image sequence u and the motion field v and ask for a suitable approximation of the above model. To gain more flexibility and, in addition, to incorporate a simple multiscale into the model, we propose here a phase field formulation (2.2) in the spirit of Ambrosio and Tortorelli [2]. Let us note that in [3] Aubert, Deriche, and Kornprobst already proposed considering this type of phase field approximation for the regularization of the motion field. We introduce

Copyright © by SIAM. Unauthorized reproduction of this article is prohibited.

an auxiliary variable ζ—the phase field—describing the edge set S. Away from S we aim for $\zeta \approx 1$, and on S the phase field ζ should vanish. As in the original Ambrosio–Tortorelli model, a scale parameter ϵ controls the thickness of the region with small phase field values. We consider the following energy functionals in the Mumford–Shah optical flow model (4.1):

$$E^{\epsilon}_{\mathrm{fid},u}[u] = \int_D \frac{\lambda_u}{2}(u-u_0)^2 \,\mathrm{d}\mathcal{L}, \tag{5.1}$$

$$E^{\epsilon}_{\mathrm{fid},w}[u,w] = \int_D \frac{\lambda_w}{2}\left(w \cdot \nabla_{(t,x)} u\right)^2 \mathrm{d}\mathcal{L}, \tag{5.2}$$

$$E^{\epsilon}_{\mathrm{reg},u}[u,\zeta] = \int_D \frac{\mu_u}{2}(\zeta^2 + k_\epsilon)\left|\nabla_{(t,x)} u\right|^2 \mathrm{d}\mathcal{L}, \tag{5.3}$$

$$E^{\epsilon}_{\mathrm{phase}}[\zeta] = \int_D \left(\nu\epsilon\left|\nabla_{(t,x)}\zeta\right|^2 + \frac{\nu}{4\epsilon}(1-\zeta)^2\right) \mathrm{d}\mathcal{L}. \tag{5.4}$$

These energy contributions control the approximation of the initial image u_0 (5.1) and the optical flow constraints (5.2), the regularity of u (5.3), and the shape of the phase field ζ (5.4). Here, as in the original model, $k_\epsilon = o(\epsilon) > 0$ is a "safety" coefficient, which is needed later to establish existence of solutions of our approximate problem. Still missing is a regularity term for the motion field corresponding to the fourth energy term in the Mumford–Shah model (4.1). If we would consider in a straightforward way the integral

$$\tilde{E}^{\epsilon}_{\mathrm{reg},w}[w,\zeta] = \int_D \frac{\mu_w}{2}(\zeta^2 + k_\epsilon)\left|\nabla_{(t,x)} w\right|^2 \mathrm{d}\mathcal{L}, \tag{5.5}$$

the motion field will form approximate jumps on S but without any coupling of a concentrated motion constraint on S and the motion field in homogeneous regions on the image sequence. Figure 8.1 clearly outlines this drawback in the case of a circle with constant white image intensity inside moving on a textured background. As an alternative one might want to decouple the scales for image edges and motion edges introducing a second phase field with a much finer scale parameter $\tilde{\epsilon} \ll \epsilon$ for the representation of motion singularities. But this is not very practical, taking into account a suitable discretization on digital images with limited pixel resolution. Here the parameter ϵ is already in the range of the pixel size. Furthermore, in case of finite energy we would obtain motion fields w bounded in $W^{1,2}$, which is not sufficient to ensure compactness of the optical flow integrand in (5.2). Thus, to allow for piecewise smooth motion fields and to enable an extension of motion velocities first concentrated on edges via the variational approach, we consider

$$E^{\epsilon}_{\mathrm{reg},w}[w,\zeta] = \int_D \frac{\mu_w}{q}\left|P_\delta[\zeta]\nabla_{(t,x)} w\right|^q \mathrm{d}\mathcal{L}. \tag{5.6}$$

Here, the following properties are encoded in the operator $P_\delta[\zeta]$:

- Close to the edges, where $\zeta \le \theta^-$ for some θ^- with $0 < \theta^- < 1$, $P_\delta[\zeta]$ should behave like the original edge indicator ζ^2 proposed by Ambrosio and Tortorelli [2].
- Away from the edges, where $\zeta \ge \theta^+$ for $\theta^- < \theta^+ < 1$, $P_\delta[\zeta]$ is expected to be the identity matrix, which enforces an isotropic smoothness modulus for the motion field w.

Copyright © by SIAM. Unauthorized reproduction of this article is prohibited.

- In the spirit of the classical approach by Nagel and Enkelmann [25], $P_\delta[\zeta]$ will be an (approximate) projection onto level sets of the phase field function in the intermediate region. These level sets are surfaces approximately parallel to the edge set in space-time. Thus, information on the optical flow is mediated along the edge set, without a coupling across edge surfaces.

An explicit definition for $P_\delta[\zeta]$ fulfilling these properties is

$$P_\delta[\zeta] = \alpha(\zeta^2)\left(\mathbb{1} + k_\epsilon - \beta(\zeta^2)\frac{\nabla_{(t,x)}\zeta}{\left|\nabla_{(t,x)}\zeta\right|_\delta} \otimes \frac{\nabla_{(t,x)}\zeta}{\left|\nabla_{(t,x)}\zeta\right|_\delta}\right),$$

where $|z|_\delta = (|z|^2 + \delta^2)^{\frac{1}{2}}$ represents a regularized normal. Furthermore, $\alpha : \mathbb{R} \to \mathbb{R}_0^+$ and $\beta : \mathbb{R} \to \mathbb{R}_0^+$ are continuous blending functions, with

$$\alpha(s) = \max\left(0, \min\left(1, \frac{s}{\theta^-}\right)\right) + k_\epsilon, \quad \beta(s) = \max\left(0, \min\left(1, 1 - \frac{s}{\theta^+}\right)\right).$$

Concerning algebraic notation, $\nabla_{(t,x)}w(t,x)$ is a $(d+1)^2$ matrix and thus $P_\delta[\zeta]\nabla_{(t,x)}w$ represents the matrix product. We consider the Frobenius norm of matrices, given by $|A| = \sqrt{\mathrm{tr}(A^T A)}$. Suitable choices for the parameters are $\theta^+ = 0.8$ and $\theta^- = 0.0025$. For vanishing ϵ and a corresponding steepening of the slope of u, this operator basically leads to a separated diffusion on both sides of S in the relaxation of the energy.

Let us recall that the energies $E^\epsilon_{\mathrm{reg},u}, E^\epsilon_{\mathrm{phase}}$ and the term $E^\epsilon_{\mathrm{fid},u}$ are identical to those in the original Ambrosio–Tortorelli approach (see above). In addition, we ask for an optical flow field w according to the optical flow constraint encoded in $E^\epsilon_{\mathrm{fid},w}$ (cf. Figure 8.1 for a first test case). At the same time, this term implies a strong coupling of the image intensities along motion trajectories—which turns into a flow-aligned diffusion in the corresponding Euler–Lagrange equations—for the benefit of a more robust denoising and edge detection. Figure 8.2 shows an example where a completely destroyed time step in the image sequence is recovered by this enhanced diffusion along motion trajectories. Due to the regularity energy $E^\epsilon_{\mathrm{reg},w}$ this motion field is isotropically smooth away from the approximate jump set of u, and the smoothness modulus is characterized by a successively stronger anisotropy along level sets of u while approaching the approximate jump set. The energy term $E^\epsilon_{\mathrm{reg},w}$ (5.6) which we consider for the regularization of the motion field is very similar to the corresponding smoothness term in the classical approach by Nagel and Enkelmann [25], where tangential diffusion is steered by the local structure tensor. In the above multiscale approach no additional prefiltering of the image sequence in terms of a structure tensor is required.

The projection operator $P_\delta[\zeta]$ couples the smoothness of the motion field w to the image geometry, which in fact is very beneficial for the purpose of piecewise smooth motion extraction. The reverse coupling, which would try to align tangent spaces of level sets of u to the motion field, is not required and might even be misleading for our actual goal. The optical flow term in the fidelity energy $E^\epsilon_{\mathrm{fid},w}$ already couples image sequence gradients to the motion field in a direct way. Hence, we don't ask for global minimizers of the sum of all energies but formulate the phase field approximation problem as follows.

DEFINITION 5.1 (solution of the phase field model). *Let $u_0 : D \to \mathbb{R}$ be a noisy space-time image, and let $v_\delta \in W^{1,q}(D, \mathbb{R}^d)$ be boundary data for the velocity field. A space-time image $u \in W^{1,2}(D, \mathbb{R})$, a motion field $w = (1, v + v_\delta)$, with $v \in W_0^{1,q}(D, \mathbb{R}^d)$, and a phase field $\zeta \in W^{1,2}(D, \mathbb{R})$ is called a solution of the phase*

Copyright © by SIAM. Unauthorized reproduction of this article is prohibited.

field model if u and ζ minimize the restricted energy

$$E_w[u,\zeta] := E^\epsilon_{\mathrm{fid},u}[u] + E^\epsilon_{\mathrm{fid},w}[u,w] + E^\epsilon_{\mathrm{reg},u}[u,\zeta] + E^\epsilon_{\mathrm{phase}}[\zeta] \tag{5.7}$$

for fixed w in $W^{1,2}(D,\mathbb{R}^{d+1})$, and if the motion field w minimizes the global energy

$$E^\epsilon_{\mathrm{global}}[u,w,\zeta] = E^\epsilon_{\mathrm{fid},u}[u] + E^\epsilon_{\mathrm{fid},w}[u,w] + E^\epsilon_{\mathrm{reg},u}[u,\zeta] + E^\epsilon_{\mathrm{reg},w}[w,\zeta] + E^\epsilon_{\mathrm{phase}}[\zeta] \tag{5.8}$$

for fixed $u,\zeta \in W^{1,2}(D,\mathbb{R})$.

In the Mumford–Shah optical flow model (4.1) the edge set S describes the discontinuities of u and w simultaneously. With the splitting introduced in the definition, we obtain a decoupling of the edge sets. Still the flow field w is smoothed along edges of u. But edges in w will not affect the phase field ζ and thus edges of u. Altogether the set of edges of w will be a subset of the edge set of u

REMARK 5.2. *The definition of u and ζ as the minimizer of a restricted functional is not only sound with respect to the applications. Indeed, a simultaneous relaxation of the global energy with respect to all unknowns is theoretically questionable. In fact, $E^\epsilon_{\mathrm{reg},w}$ is not convex in ζ, and we cannot expect this energy contribution to be lower semicontinuous on a suitable set of admissible functions. With the above notion of solutions the direct method in the calculus of variations can be applied, and in particular one observes compactness of the sequence of phase fields associated with a minimizing sequence of image sequences and motion fields (cf. the proof below).*

THEOREM 5.3 (existence of solutions). *Suppose that $d+1 < q < \infty$ and $\lambda_u, \lambda_w, \mu_u, \mu_w, \nu, \epsilon > 0$, and let $k_\epsilon > 0$. Then there exists a solution (u,w,ζ) of the phase field problem introduced in Definition* 5.1.

Proof. At first, we rewrite the phase field approach as an energy minimization problem, which later allows us to apply the direct method from the calculus of variations. For fixed w the energy functional $E_w[u,\zeta]$ (5.7) is strictly convex. By the direct method we obtain a unique minimizer. So let us denote by $(u[w],\zeta[w])$ this minimizer in $W^{1,2}(D,\mathbb{R}) \times W^{1,2}(D,\mathbb{R})$ of the quadratic energy functional $E_w[u,\zeta]$ for fixed $u \in W^{1,2}(D,\mathbb{R})$. The minimizing phase field is given as the weak solution of the corresponding Euler–Lagrange equation

$$-\epsilon\Delta\zeta + \frac{1}{4\epsilon}\zeta = f[u,\zeta] := \frac{1}{4\epsilon} - \frac{\mu_u}{2\nu}\left|\nabla_{(t,x)}u\right|^2\zeta. \tag{5.9}$$

Applying the weak maximum principle we observe that $\overline{\zeta} \equiv 1$ is a supersolution and $\underline{\zeta} \equiv 0$ a subsolution. Thus, $\zeta[w]$ is uniformly bounded, i.e., $0 \le \zeta[w] \le 1$.

Given $(u[w],\zeta[w])$ we consider the global energy $E^\epsilon_{\mathrm{global}}$ solely as a functional of the motion field $w = (1,v)$:

$$E[w] = E^\epsilon_{\mathrm{global}}[u[w],w,\zeta[w]]$$

on the admissible set

$$\mathcal{A} := \{w \mid w = (1, v+v_\delta),\ v \in W^{1,q}_0(D,\mathbb{R}^{d+1})\},$$

and we define $\underline{E} := \inf_{w\in\mathcal{A}} E[w]$. Testing the energy at $u \equiv 0$, $\zeta \equiv 0$, and $w = (1,v_\delta)$ we observe that $\underline{E} \le \frac{\lambda_u}{2}|u_0|^2_{L^2} + \frac{\mu_w}{q}\left|\nabla_{(t,x)}v_\delta\right|^q_{L^q} < \infty$. Let us consider a minimizing sequence $\left(w^k\right)_{k=1,\dots,\infty}$ in $\mathcal{A}$ with $E[w^k] \to \underline{E}$ for $k \to \infty$. We set $u^k = u[w^k]$ and

Copyright © by SIAM. Unauthorized reproduction of this article is prohibited.

$\zeta^k = \zeta[w^k]$ and estimate the energy E_{global} as

$$E_{\text{global}}[u,w,\zeta] \geq \frac{\lambda_u}{4}\left(|u|_{L^2}^2 - 2\,|u_0|_{L^2}^2\right) + \frac{\mu_u k_\epsilon}{2}\left|\nabla_{(t,x)}u\right|_{L^2}^2 + \frac{\mu_w k_\epsilon}{q}\left|\nabla_{(t,x)}w\right|_{L^q}^q + \frac{\nu}{4\epsilon}\left(|\zeta|_{L^2}^2 - 2\mathcal{L}(D)\right) + \nu\epsilon\left|\nabla_{(t,x)}\zeta\right|_{L^2}^2,$$

where $\mathcal{L}(D)$ denotes the Lebesgue measure of D. From this, we deduce that $(u^k)_k$ and $(\zeta^k)_k$ are bounded in $W^{1,2}(D,\mathbb{R})$ and, taking into account the boundary conditions, that $(w^k)_k$ is bounded in $W^{1,q}(D,\mathbb{R})$. Hence, we can extract a weakly converging subsequence again denoted by $(u^k,w^k,\zeta^k)_k$ having the weak limit (u,w,ζ). From the Sobolev embedding theorem and the assumption $q > d+1$ we derive that w^k strongly converges in L^∞. Furthermore, the corresponding sequence $(\zeta^k)_k$ of phase field functions $\zeta^k := \zeta[w^k]$ are weak solutions of $-\epsilon\Delta\zeta^k + \frac{1}{4\epsilon}\zeta^k = f^k$ (cf. (5.9)). From the bounds on ζ^k in L^∞ and on u^k in $W^{1,2}$ we obtain that $f^k = f[u^k,\zeta^k]$ is uniformly bounded in L^1. This observation allows us to apply a compensated compactness result to verify that $\nabla_{(t,x)}\zeta^k$ converges to $\nabla_{(t,x)}\zeta$ a.e. This is proven for the equation $-\Delta\zeta = f$ on the space $W_0^{1,2}$ in [34, Chap. I, Thm. 3.4], but can easily be generalized for equations of type $-\Delta\zeta + \zeta = f$ on $W^{1,2}$. The matrix-valued function $P_\delta[\cdot]$ is continuous and bounded. Hence, we obtain that $P_\delta[\zeta^k] \to P_\delta[\zeta]$ a.e. for $k\to\infty$. For later use, we define the constants $C_u = \sup_{k=1,\dots,\infty}\left|\nabla_{(t,x)}u^k\right|_{L^2}$ and $C_w = \sup_{k=1,\dots,\infty}\max\left\{\left|w^k\right|_{L^\infty},\left|\nabla_{(t,x)}w^k\right|_{L^q}\right\}$.

Next, we verify that $u = u[w]$ and $\zeta = \zeta[w]$. Indeed, taking into account the lower semicontinuity of E_w and the modulus of continuity with respect to w we can estimate

$$\begin{aligned}
E_w[u,\zeta] &\leq \liminf_{k\to\infty} E_{w^k}[u^k,\zeta^k]\\
&\leq \liminf_{k\to\infty} E_{w^k}[\tilde u,\tilde\zeta]\\
&\leq E_w[\tilde u,\tilde\zeta] + \liminf_{k\to\infty}\left(\left|w^k\cdot\nabla_{(t,x)}\tilde u\right|_{L^2}^2 - \left|w\cdot\nabla_{(t,x)}\tilde u\right|_{L^2}^2\right)\\
&\leq E_w[\tilde u,\tilde\zeta] + 2C_w\left|\nabla_{(t,x)}\tilde u\right|_{L^2}^2 \liminf_{k\to\infty}\left|w-w^k\right|_{L^\infty}
\end{aligned}$$

for any $\tilde u,\tilde\zeta \in W^{1,2}(D,\mathbb{R})$. From the L^∞ convergence of w^k to w, we immediately obtain that $E_w[u,\zeta] \leq E_w[\tilde u,\tilde\zeta]$. Thus, by definition $u = u[w]$ and $\zeta = \zeta[w]$. Based on these preliminaries, we are able to prove weak lower semicontinuity of the energy. For this we assume without loss of generality that

$$E[w^k] \leq \underline{E} + \rho, \quad \left|P_\delta[\zeta^k] - P_\delta[\zeta]\right|_{L^\infty} \leq \rho, \quad \left|w^k - w\right|_{L^\infty} \leq \rho$$

for a fixed and small constant $\rho > 0$. Applying Mazur's lemma we obtain a sequence of convex combinations

$$\left(\sum_{i=1,\dots,k}\lambda_i^k(u^i,w^i,\zeta^i)\right)_k, \quad \text{with}\ \sum_{i=1,\dots,k}\lambda_i^k = 1, \quad \lambda_i^k \geq 0,$$

converging strongly to (u,w,ζ) in $W^{1,2}(D,\mathbb{R})\times W^{1,2}(D,\mathbb{R}^{d+1})\times W^{1,2}(D,\mathbb{R})$. Finally, taking into account convexity properties of the integrands, Fatou's lemma, and

Copyright © by SIAM. Unauthorized reproduction of this article is prohibited.

the modulus of continuity of $E_{\mathrm{fid},u}$, $E_{\mathrm{fid},w}$, and $E_{\mathrm{reg},w}$ with respect to w and $P_\delta[\zeta]$, respectively, we estimate (using Einstein's summation convention)

$$
\begin{aligned}
E[w] &= E_{\mathrm{global}}[u[w], w, \zeta[w]] = E_{\mathrm{global}}[u, w, \zeta] \\
&= \int_D \frac{\lambda_u}{2} \left(\liminf_{k\to\infty} \lambda_i^k u^i - u_0 \right)^2 + \frac{\lambda_w}{2} \left| \liminf_{k\to\infty} w \cdot \left(\lambda_i^k \nabla_{(t,x)} u^i \right) \right|^2 \mathrm{d}\mathcal{L} \\
&\qquad + \int_D \frac{\mu_u}{2} (\zeta^2 + k_\epsilon) \left| \liminf_{k\to\infty} \lambda_i^k \nabla_{(t,x)} u^i \right|^2 + \frac{\mu_w}{q} \left| \liminf_{k\to\infty} P_\delta[\zeta] \lambda_i^k \nabla_{(t,x)} w^i \right|^q \mathrm{d}\mathcal{L} \\
&\qquad + \int_D \left(\nu\epsilon \left| \liminf_{k\to\infty} \lambda_i^k \nabla \zeta^i \right|^2 + \frac{\nu}{4\epsilon} \left(1 - \liminf_{k\to\infty} \lambda_i^k \zeta^i \right)^2 \right) \mathrm{d}\mathcal{L} \\
&\leq \int_D \frac{\lambda_u}{2} \liminf_{k\to\infty} \lambda_i^k \left(\left(u^i - u_0 \right)^2 + \frac{\lambda_w}{2} \left| w \cdot \left(\nabla_{(t,x)} u^i \right) \right|^2 \right) \mathrm{d}\mathcal{L} \\
&\qquad + \int_D \liminf_{k\to\infty} \lambda_i^k \left(\frac{\mu_u}{2} (\zeta^2 + k_\epsilon) \left| \nabla_{(t,x)} u^i \right|^2 + \frac{\mu_w}{q} \left| P_\delta[\zeta] \nabla_{(t,x)} w^i \right|^q \right) \mathrm{d}\mathcal{L} \\
&\qquad + \int_D \liminf_{k\to\infty} \lambda_i^k \left(\nu\epsilon \left| \nabla_{(t,x)} \zeta^i \right|^2 + \frac{\nu}{4\epsilon} (1 - \zeta^i)^2 \right) \mathrm{d}\mathcal{L} \\
&\leq \liminf_{k\to\infty} \lambda_i^k E[u^i, w^i] + \frac{\lambda_w}{2} \sup_{i=1,\dots,\infty} \left(\left| w^i \cdot \nabla_{(t,x)} u^i \right|_{L^2}^2 - \left| w \cdot \nabla_{(t,x)} u^i \right|_{L^2}^2 \right) \\
&\qquad + \frac{\mu_w}{q} \sup_{i=1,\dots,\infty} \left(\left| P_\delta[\zeta^i] \nabla_{(t,x)} w^i \right|_{L^q}^q - \left| P_\delta[\zeta] \nabla_{(t,x)} w^i \right|_{L^q}^q \right) \\
&\leq \underline{E} + \lambda_w C_w C_u^2 \sup_{i=1,\dots,\infty} \left| w^i - w \right|_{L^\infty} + \mu_w C_w^q \sup_{i=1,\dots,\infty} \left(\left| P_\delta[\zeta^i] - P_\delta[\zeta] \right|_{L^\infty} \right) \\
&\leq \underline{E} + \rho + \lambda_w C_w C_u^2 \rho + \mu_w C_w^q \rho.
\end{aligned}
$$

This estimate holds for any $\rho \geq 0$. Thus, we obtain $E[w] \leq \underline{E}$, which implies that w is a minimizer of the energy E, and hence (u, w, ζ) is a solution of our phase field problem. ∎

REMARK 5.4. *The above problem formulation is not only sound with respect to the actual modeling, but it will also allow a simple relaxation approach (see below). Indeed, on all tested data sets we obtain convergence in few iterations (*10–15*).*

Applying formal asymptotics, one observes that the phase field approach proposed here indeed converges to the above Mumford–Shah model. For small ϵ we expect a steepening of the gradient u on a stripe of thickness ϵ around the edge set. The phase field ζ will approximate 1 away from a shrinking neighborhood of the edge surface. For $\epsilon \to 0$ we expect to observe convergence of $E_{\mathrm{reg},u}$ and $E_{\mathrm{reg},w}$ to $\int_{D\setminus S} \frac{\mu_u}{2} \left| \nabla_{(t,x)} u \right|^2 + \frac{\mu_w}{q} \left| \nabla_{(t,x)} u \right|^q \mathrm{d}\mathcal{L}$ and of $E_{\mathrm{phase}}^\epsilon$ to $\mathcal{H}^d(S)$. Under these assumptions on the qualitative behavior $\int_D (w \cdot \nabla_{(t,x)} u)^2 \, \mathrm{d}\mathcal{L}$ converges to the second term of E_{MSopt}, whereas on the edge surface one observes a concentration of energy on the jump set and which scales like $O(\epsilon^{-1})$. Thus, we observe that in the limit we reproduce our optical flow constraint $n_S \cdot (w^+ + w^-) = 0$ from the sharp-interface Mumford–Shah approach. A rigorous validation of this limit behavior in terms of Γ-convergence is still open. For results on Γ-convergence for the optical flow problem in the context of TV type models we refer to [4, 22].

6. Variations of the energy and an algorithm. In what follows, we will consider the Euler–Lagrange equations of the above energies. Thus, we need to compute the variations of the energy contributions with respect to the involved unknowns

Copyright © by SIAM. Unauthorized reproduction of this article is prohibited.

u, w, ζ. The variation of an energy E in direction ζ with respect to a parameter function z will be denoted by $\langle \delta_z E, \zeta \rangle$. For the ease of implementation we consider the case $q = 2$. Using straightforward differentiation for sufficiently smooth u, w, ζ and initial data u_0 we obtain

$$
\begin{aligned}
\langle \delta_u E^\epsilon_{\mathrm{fid},u}[u], \vartheta \rangle &= \int_D \lambda_u (u - u_0)\, \vartheta \,\mathrm{d}\mathcal{L}, \\
\langle \delta_u E^\epsilon_{\mathrm{fid},w}[u, w], \vartheta \rangle &= \int_D \lambda_w (\nabla_{(t,x)} u \cdot w)(\nabla_{(t,x)} \vartheta \cdot w)\,\mathrm{d}\mathcal{L}, \\
\langle \delta_w E^\epsilon_{\mathrm{fid}}[u, w], \psi \rangle &= \int_D \lambda_w (\nabla_{(t,x)} u \cdot w)(\nabla_{(t,x)} u \cdot \psi)\,\mathrm{d}\mathcal{L}, \\
\langle \delta_u E^\epsilon_{\mathrm{reg},u}[u, \zeta], \vartheta \rangle &= \int_D \mu_u (\zeta^2 + k_\epsilon) \nabla_{(t,x)} u \cdot \nabla_{(t,x)} \vartheta \,\mathrm{d}\mathcal{L}, \\
\langle \delta_\zeta E^\epsilon_{\mathrm{reg},u}[u, \zeta], \xi \rangle &= \int_D \mu_u \zeta \left| \nabla_{(t,x)} u \right|^2 \xi \,\mathrm{d}\mathcal{L}, \\
\langle \delta_w E^\epsilon_{\mathrm{reg},w}[w, \zeta], \psi \rangle &= \int_D \mu_w P_\delta[\zeta] \nabla_{(t,x)} w : \nabla_{(t,x)} \psi \,\mathrm{d}\mathcal{L}, \\
\langle \delta_\zeta E^\epsilon_{\mathrm{phase}}[\zeta], \xi \rangle &= \int_D 2\nu\epsilon \nabla_{(t,x)} \zeta \cdot \nabla_{(t,x)} \xi \,\mathrm{d}\mathcal{L} + \int_D \frac{\nu}{2\epsilon} (\zeta - 1) \xi \,\mathrm{d}\mathcal{L}
\end{aligned}
\tag{6.1}
$$

for scalar test functions ξ, ϑ and velocity-type test functions ψ with the structure $\psi = (0, \pi)$. Here, we use the notation $A : B := \mathrm{tr}(B^T A)$. Now, summing up the different terms as in (5.7) and integrating by parts, we end up with the system of PDEs

$$
-\operatorname{div}_{(t,x)} \left(\frac{\mu_u}{\lambda_u} (\zeta^2 + k_\epsilon) \nabla_{(t,x)} u + \frac{\lambda_w}{\lambda_u} w (\nabla_{(t,x)} u \cdot w) \right) + u = u_0, \tag{6.2}
$$

$$
-\epsilon \Delta_{(t,x)} \zeta + \left(\frac{1}{4\epsilon} + \frac{\mu_u}{2\nu} \left| \nabla_{(t,x)} u \right|^2 \right) \zeta = \frac{1}{4\epsilon}, \tag{6.3}
$$

$$
-\frac{\mu_w}{\lambda_w} \operatorname{div}_{(t,x)} \left(P_\delta[\zeta] \nabla_{(t,x)} v \right) + (\nabla_{(t,x)} u \cdot v) \nabla_x u = 0 \tag{6.4}
$$

as the Euler–Lagrange equations characterizing the necessary conditions for a solution (u, w, ζ) of the above-stated phase field approach. Let us emphasize that with the full Euler–Lagrange equations, characterizing a global minimizer of the energy would in addition involve variations of $E_{\mathrm{reg},w}$ with respect to ζ. However, as described in section 5, we do not consider this variation, since it would add a coupling of the edges of the flow field to the edges of the image. Thus, the PDE system (6.2)–(6.4) directly corresponds to our notion of solution specified in Definition 5.1.

For Neumann boundary conditions (which we actually consider in the application) the Euler–Lagrange equation in w is not guaranteed to be coercive in $W^{1,q}$. Indeed, the optical flow term $w \cdot \nabla_{(t,x)} u$ represents a pointwise rank-1 condition, and it is not known a priori that "sufficiently many" of these conditions, in the sense of the Lebesgue measure, are assembled in the image while integrating this term. To remedy this degeneracy, we consider a gradient descent of (6.4)

$$
\partial_s v - \frac{\mu_w}{\lambda_w} \operatorname{div}_{(t,x)} \left(P_\delta[\zeta] \nabla_{(t,x)} v \right) + (\nabla_{(t,x)} u \cdot w) \nabla_x u = 0. \tag{6.5}
$$

Copyright © by SIAM. Unauthorized reproduction of this article is prohibited.

Consequently, the matrices resulting from a discretization are well conditioned and the corresponding systems can be solved easily (see section 7).

Inspired by Ambrosio and Tortorelli, we propose the following iterative algorithm for the solution of the phase field problem with $q = 2$:

Step 0. Initialize $u = u_0$, $\zeta \equiv 1$, and $w \equiv (1, 0)$.
Step 1. Solve (6.2) for fixed w, ζ.
Step 2. Solve (6.3) for fixed u, w.
Step 3. Compute one step of the gradient descent (6.5) for fixed u, ζ.
Step 4. Return to Step 1.

Steps 1 and 2 of the algorithm consist of a consecutive solution of linear PDEs. Let us note that we use a time step control for the gradient descent in Step 3. Alternatively we might iterate first Steps 1 and 2 until convergence, and then in another iteration we would consider the identification of the motion field w. Even though this second variation seems to be closer to our definition of solutions of the phase field problem, the above algorithm converges to the same solution in the applications we have considered. Our algorithm can be seen as a diagonal scheme, where the iteration of Steps 1 and 2 and the gradient descent iteration in Step 3 are intertwined.

7. Finite element discretization. We proceed similarly to the finite element method proposed by Bourdin and Chambolle [5, 6] for the phase field approximation of the Mumford–Shah functional, which is an extension of the approach first presented by Chambolle and Dal Maso [10].

To solve the above system of PDEs we suppose $[0, T] \times \Omega$ to be overlaid by a regular hexahedral grid. In the following, the spatial and temporal grid width are denoted by h and τ, respectively. Hence, image frames are at a distance of τ and pixels of each frame are placed on a regular mesh with grid size h.

On this hexahedral grid we consider the space of piecewise trilinear continuous functions $\mathcal{V}$ and ask for discrete functions $U, Z \in \mathcal{V}$ and $V \in \mathcal{V}^2$, such that discrete and weak counterparts of the Euler–Lagrange equations (6.2), (6.3), and (6.4) are fulfilled. This leads to the solution of systems of linear equations for the vectors of the nodal values of the unknowns U, Z, V. We refer to the appendix for a detailed description of the matrices and the resulting systems of equations. A careful implementation is required to ensure an efficient method. For a time-space volume of K time steps and images of $N \times M$ pixels, the finite element matrices for U and Z have $N\,M\,K\,C$ entries, where $C = 27$ is the number of nonzero entries per row, equal to the number of couplings of a node. The finite element matrix for V has four times more elements, as V is a two-dimensional vector. Data-sets of up to $K = 10$ frames of $N = 500$, $M = 320$ pixels can be treated by standard hardware with less than 1GB memory. The linear systems of equations are solved applying a classical conjugate gradient method. For the pedestrian sequence (Figure 8.5), one such iteration takes 47 seconds on a Pentium IV PC at 1.8 GHz running Linux. The complete method typically converges after 10–15 such iterations. To treat large video sequences, we typically consider a window of $K = 6$ frames, to avoid boundary effects, and then shift this window successively in time.

In Figure 7.1 we have depicted the progression of the various components of the energy $E^{\epsilon}_{\text{global}}$ for the taxi sequence shown in Figure 8.6. The rapid decay of the global energy in the first steps of the algorithm is clearly visible. While the image fidelity $E^{\epsilon}_{\text{fid}}$ and its regularity $E^{\epsilon}_{\text{reg},u}$ decay, the other parts of the energy increase. Obviously this is the case, because we are starting with constant initial values $\zeta = 0$ and $w = (1, 0)$.

Copyright © by SIAM. Unauthorized reproduction of this article is prohibited.

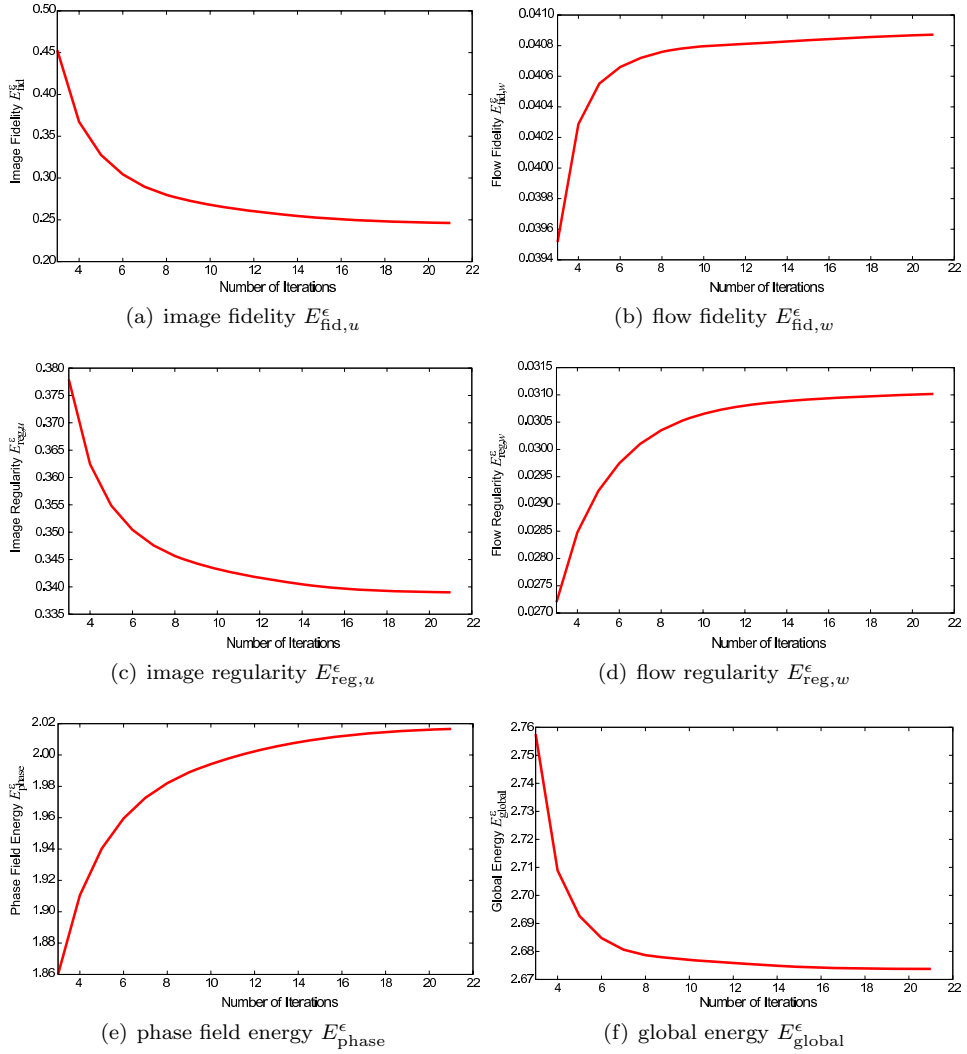

(a) image fidelity $E^{\epsilon}_{\text{fid},u}$ (b) flow fidelity $E^{\epsilon}_{\text{fid},w}$

(c) image regularity $E^{\epsilon}_{\text{reg},u}$ (d) flow regularity $E^{\epsilon}_{\text{reg},w}$

(e) phase field energy $E^{\epsilon}_{\text{phase}}$ (f) global energy $E^{\epsilon}_{\text{global}}$

FIG. 7.1. *For the example presented in Figure* 8.6 *(bottom row) we show the progression of the various energy contributions during the solution iteration. The decay of the global energy can be seen in the lower right plot* (f).

8. Results and discussion. We present here several results of the proposed method for two-dimensional image sequences. In the considered examples, the parameter setting $\epsilon = h/4$, $\mu_u = h^{-2}$, $\mu_w = \lambda_u = 1$, $\lambda_w = 10^5 h^{-2}$, and $k_\epsilon = \epsilon$, $\delta = \epsilon$ has proven to give good results. We first consider a simple example of a white disk moving with constant speed $v = (1, 1)$ on a vaguely textured, low-contrast, dark background (Figure 8.1). Let us first consider the top row in Figure 8.1, which corresponds to the energy formulation without the projection component. A limited amount of smoothing results from the regularization energy $E^{\epsilon}_{\text{reg},u}$ (Figure 8.1(a)), which is desirable to ensure robustness in the resulting optical flow term $\nabla_{(t,x)} u \cdot w$ and removes noisy artifacts in real-world videos; see, e.g., Figures 8.4 and 8.5. The phase field clearly captures the moving object's contour. The optical flow is depicted in Figure 8.1(c) by color coding the vector directions as shown by the lower right color wheel. Clearly, the method is able to extract the uniform motion of the disc's boundary, which has a

Copyright © by SIAM. Unauthorized reproduction of this article is prohibited.

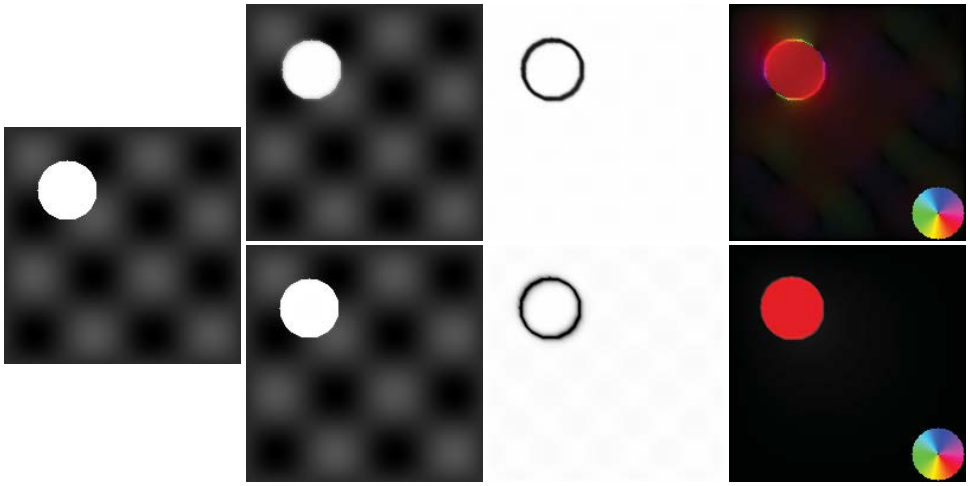

FIG. 8.1. *One frame of the test sequence (left) and corresponding smoothed images* (a)*, phase field* (b)*, optical flow (color coded)* (c)*. Top row: Energy formulation without projection. Bottom row: energy formulation with projection.*

high image contrast. The optical flow information, available only on the motion edges (black in Figure 8.1(b)), is propagated only to a limited extent into the informationless area inside the moving disk. Indeed, we notice that the model with the standard regularity term for w (5.5) is not able to diffuse the optical flow information, concentrated on the motion edges, in order to completely and uniformly fill in the moving circle.

In the bottom row of Figure 8.1, the same example is shown, this time run with the energy formulation including the projection term. We now clearly see a perfect reconstruction of the optical flow (Figure 8.1(c), bottom row) also inside the nontextured moving disc.

In the next example we revisit this simple image sequence of the moving circle. This time we have added noise to the sequence. At the same time we have completely destroyed the information of one frame of the sequence. In Figure 8.2 we show the results for frames 3 and 9–11, where frame 10 has been completely destroyed. From the images we see that the phase field detects the missing circle in the destroyed frame as a temporal edge surface in the sequence. Indeed the ζ drops down to zero in the temporal vicinity of the destroyed frame. This is still visible in the previous and the next time steps, shown in the second and third rows. But it does not hamper the restoration of the correct optical flow field shown in the fourth column. This is due to the anisotropic smoothing of information from the surrounding frames into the destroyed frame. For this example we have chosen $\epsilon = 0.4h$.

Another synthetic example is shown in Figure 8.3. This example is from the publicly available data-set collection at [11]. Here, a textured sphere spins on a textured background (Figure 8.3(a)). Again, the method is able to clearly segment the moving object from the background, even though the object does not change position. We used a phase field parameter $\epsilon = 0.15h$. The extracted optical flow clearly shows the spinning motion (Figure 8.3(d)) and the discontinuous motion field.

A first example on real video data is shown in Figure 8.4. The video shows a table tennis player whose body moves to the right while the hand goes down as he strikes the ball. This motion is well captured in the flow field (Figure 8.4(c)).

Copyright © by SIAM. Unauthorized reproduction of this article is prohibited.

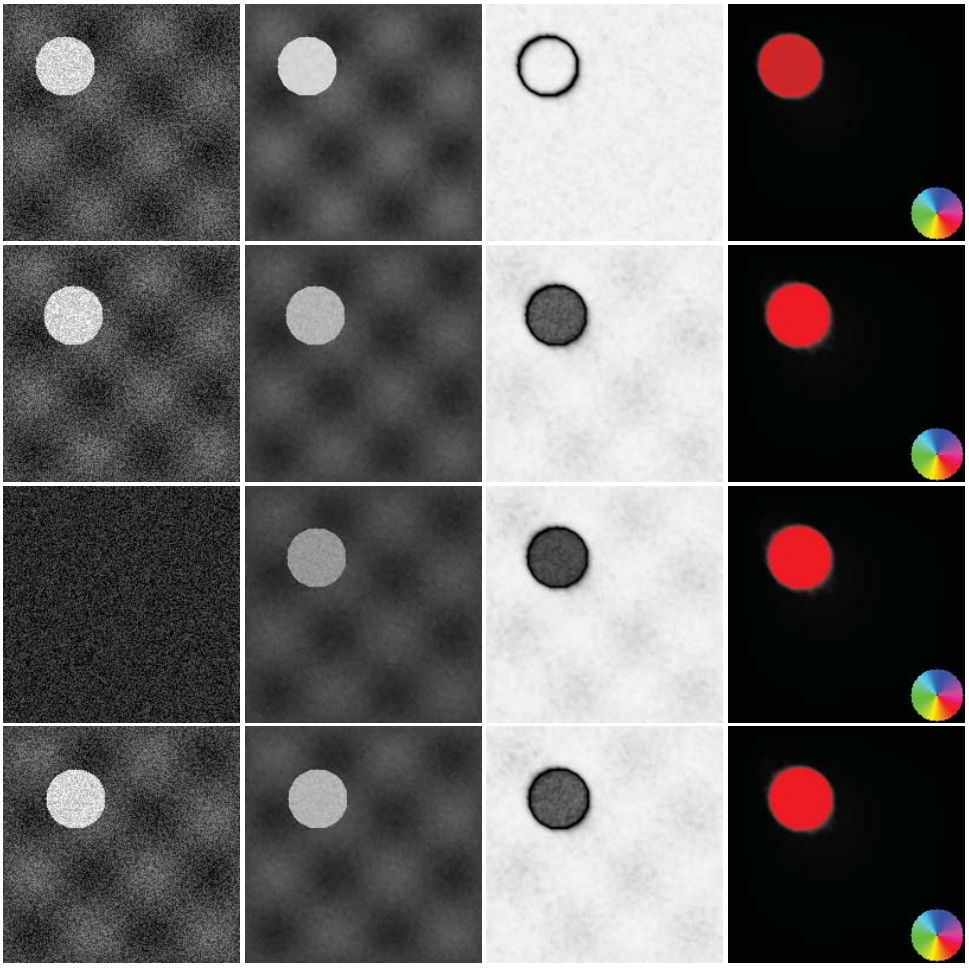

FIG. 8.2. *Noisy test sequence: From top to bottom frames* 3 *and* 9–11 *are shown.* (a) *Original image sequence,* (b) *smoothed images,* (c) *phase field,* (d) *estimated motion (color coded).*

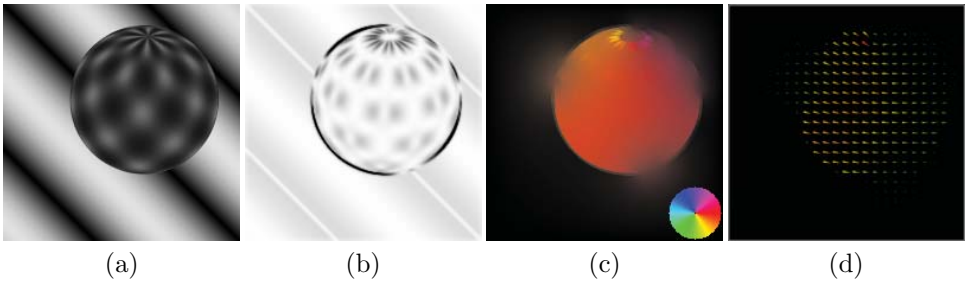

FIG. 8.3. *Rotating sphere: smoothed image* (a), *phase field* (b), *optical flow (color coded)* (c), *optical flow (vector plot, color coded magnitude)* (d).

Furthermore, we consider a complex, higher resolution video sequence, taken under outdoor conditions by a monochrome video camera. The sequence shows a group of walking pedestrians (Figure 8.5 (top)). The human silhouettes are well extracted

Copyright © by SIAM. Unauthorized reproduction of this article is prohibited.

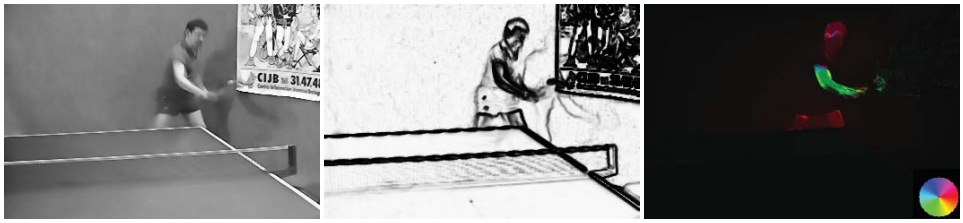

(a) (b) (c)

FIG. 8.4. *Table tennis sequence: smoothed image* (a)*, phase field* (b)*, and optical flow* (c).

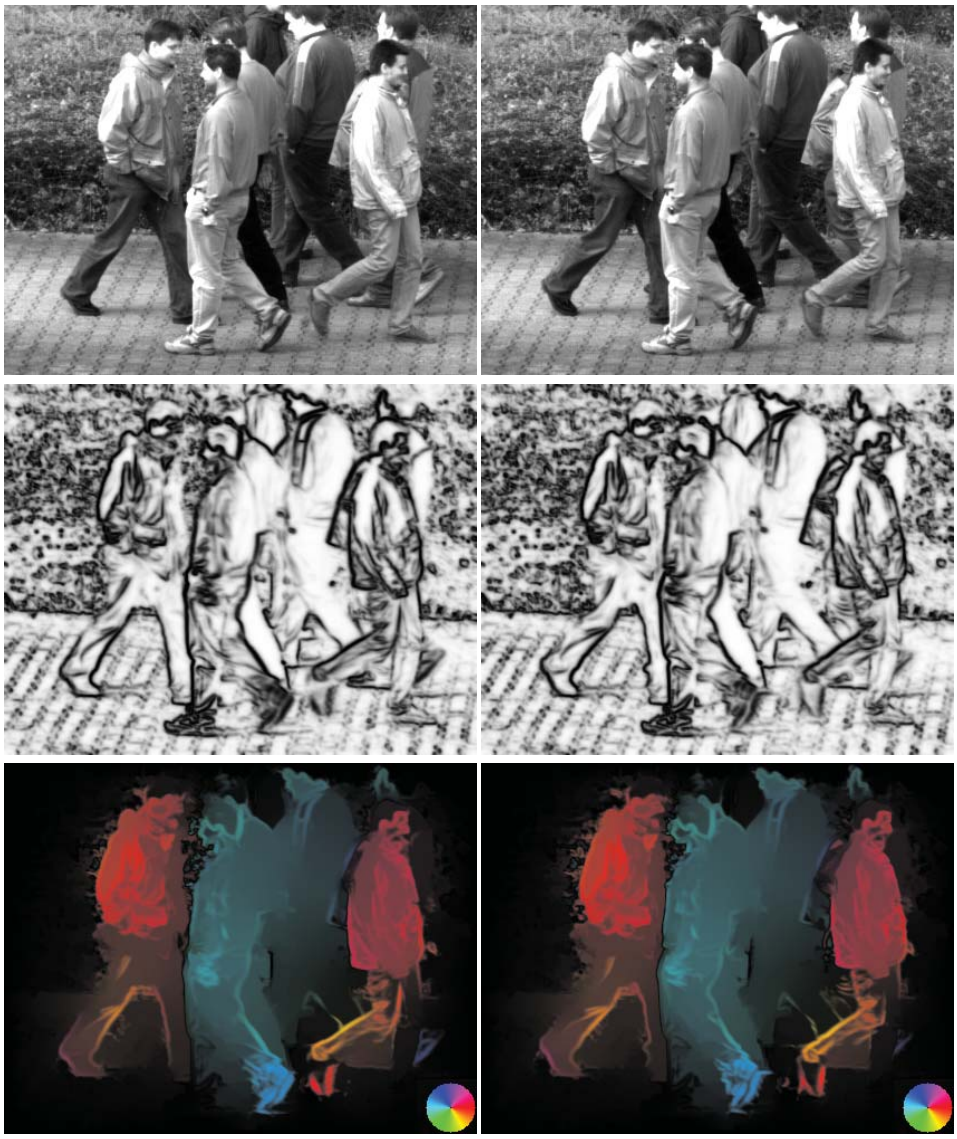

FIG. 8.5. *Pedestrian video: frames from original sequence (top), phase field (middle), and optical flow, color coded (bottom).*

Copyright © by SIAM. Unauthorized reproduction of this article is prohibited.

FIG. 8.6. *The taxi sequence. Original image (left). Flow extraction without the projection operator (top row) and with projection (bottom row). Smoothed image* (a)*, phase field* (b)*, and optical flow, color coded* (c).

and captured by the phase field (Figure 8.5 (middle)). We do not show a vector plot of the optical flow, as it is hard to interpret visually at the video sequence resolution of 640×480 pixels. However, the color-coded optical flow plot (Figure 8.5 (bottom)) shows how the method is able to extract the moving limbs of the pedestrians. The overall red and blue color corresponds to the walking directions of the pedestrians. The estimated motion is smooth inside the areas of the individual pedestrians and not smeared across the motion boundaries. In addition, the algorithm nicely segments the different moving persons. The cluttered background poses no big problem to the segmentation, nor do the edges of occluding and overlapping pedestrians, who are moving at almost the same speed.

Finally, let us note a limitation of the approach we have presented above: Let us consider the well-known Hamburg taxi video sequence, which is available from [18]. Figure 8.6 shows the taxi sequence processed both with the classical AT energy component (top row) and with our projection operator (bottom row). The progression of the various energy contributions is shown in Figure 7.1. Here we start with $u = 0$, i.e., a black image, and a zero velocity field $v = 0$. In this sequence, cars of differing image contrasts are moving. When the projection operator P_δ in our model is used (bottom row), only the central, high-contrast moving car is captured. When the operator is not used (top row), motion edges corresponding to low-contrast image edges also determine the phase field; hence the other oppositely moving cars in the bottom part of the image are captured as well and the corresponding optical flow is extracted. For all the cars in this example, the motion field is determined largely by the low-contrast shading and not only by high-contrast image edges, as was the case in the synthetic example in Figure 8.1.

Appendix. Algorithmic building blocks. In this appendix we would like to focus on the discrete version of the Euler–Lagrange equations resulting from (5.7). Let us denote by $\{\Psi_i\}_{i=1,\dots,N}$ the usual nodal basis of $\mathcal{V}$ (cf. section 7). The corresponding basis of the vector-valued discrete functions $\Psi \in \mathcal{V}^2$ is given by $\{\Psi_i e_1\}_i \cup \{\Psi_i e_2\}_i$, where $e_{1,2}$ are the standard basis vectors of $\mathbb{R}^2$: $e_1 = (1, 0)$, $e_2 = (0, 1)$. For any discrete function $Q \in \mathcal{V}$ we denote by $\overline{Q}$ the corresponding nodal vector. For discrete vector-valued functions we order the coefficients such that the e_1 coefficients are followed by the e_2 coefficients. Hence, the systems of discrete equations to be solved in

Copyright © by SIAM. Unauthorized reproduction of this article is prohibited.

the above algorithm are given in matrix vector notion as follows. We ask for solution vectors $\overline{U}, \overline{Z} \in \mathbb{R}^N$ and $\overline{V} \in \mathbb{R}^{2N}$, such that denoting $\overline{W} = (1, \overline{V})$ we have

$$(\mathbf{L}_u[W, \zeta] + \mathbf{M})\overline{U} = R_u, \tag{A.1}$$

$$(\mathbf{L}_\zeta + \mathbf{M}_\zeta[U])\overline{Z} = R_\zeta, \tag{A.2}$$

$$(\mathbf{L}_w[Z] + \mathbf{M}_w[U])\overline{V} = R_w. \tag{A.3}$$

These systems contain the matrices $\mathbf{L}_u[W, Z], \mathbf{L}_\zeta, \mathbf{M}, \mathbf{M}_\zeta[U] \in \mathbb{R}^{N\times N}$, $\mathbf{L}_w[Z], \mathbf{M}_w[U] \in \mathbb{R}^{2N\times 2N}$, $R_u, R_\zeta \in \mathbb{R}^n$, and finally $R_w \in \mathbb{R}^{2N}$, which can easily be derived from the variations of the energy (5.8). We have

$$\begin{aligned}
(\mathbf{L}_u[W, Z])_{ij} &= \int_D \frac{\mu_u}{\lambda_u}(Z^2 + k_\epsilon)\nabla_{(t,x)}\Psi_i \cdot \nabla_{(t,x)}\Psi_j \\
&\qquad + \frac{\lambda_w}{\lambda_u}(\nabla_{(t,x)}\Psi_i \cdot W)(\nabla_{(t,x)}\Psi_j \cdot W)\,\mathrm{d}\mathcal{L}, \\
\mathbf{M}_{ij} &= \int_D \Psi_i\Psi_j\,\mathrm{d}\mathcal{L}, \\
R_u &= \mathbf{M}\overline{\mathcal{I}_h u_0},
\end{aligned}$$

as well as

$$\begin{aligned}
(\mathbf{L}_\zeta)_{ij} &= \epsilon \int_D \nabla_{(t,x)}\Psi_i \cdot \nabla_{(t,x)}\Psi_j\,\mathrm{d}\mathcal{L}, \\
(\mathbf{M}_\zeta[U])_{ij} &= \int_D \left(\frac{\mu_u}{2\nu}\left|\nabla_{(t,x)}U\right|^2 + \frac{1}{4\epsilon}\right)\Psi_i\Psi_j\,\mathrm{d}\mathcal{L}, \\
(R_\zeta)_i &= \frac{1}{4\epsilon}\int_D \Psi_i\,\mathrm{d}\mathcal{L}
\end{aligned}$$

and

$$\begin{aligned}
(\mathbf{L}_w[Z])_{ikjl} &= \int_D \mu_w P_\delta[Z]\nabla_{(t,x)}\Psi_i \cdot \nabla_{(t,x)}\Psi_j\delta_{kl}\,\mathrm{d}\mathcal{L}, \\
(\mathbf{M}_w[U])_{ikjl} &= \int_D \lambda_w \partial_{x_k}U\partial_{x_l}U\,\Psi_i\Psi_j\,\mathrm{d}\mathcal{L}, \\
(R_w)_{ik} &= -\int_D \lambda_w \partial_t U\partial_{x_k}U\Psi_i\,\mathrm{d}\mathcal{L}.
\end{aligned}$$

Here, δ_{kl} is the usual Kronecker symbol, which is 1 if $k = l$ and otherwise 0. Let us remark that the integrands are piecewise polynomials of degree ≤ 2. We use a suitable quadrature rule on the hexahedra, which ensures exact integration.

REFERENCES

[1] L. Ambrosio, N. Fusco, and D. Pallara, *Functions of Bounded Variation and Free Discontinuity Problems*, Oxford University Press, New York, 2000.

[2] L. Ambrosio and V. M. Tortorelli, *On the approximation of free discontinuity problems*, Boll. Un. Mat. Ital. B (7), 6 (1992), pp. 105–123.

[3] G. Aubert, R. Deriche, and P. Kornprobst, *Computing optical flow via variational techniques*, SIAM J. Appl. Math., 60 (1999), pp. 156–182.

Copyright © by SIAM. Unauthorized reproduction of this article is prohibited.

[4] G. Aubert and P. Kornprobst, *A mathematical study of the relaxed optical flow problem in the space $BV(\Omega)$*, SIAM J. Math. Anal., 30 (1999), pp. 1282–1308.
[5] B. Bourdin, *Image segmentation with a finite element method*, M2AN Math. Model. Numer. Anal., 33 (1999), pp. 229–244.
[6] B. Bourdin and A. Chambolle, *Implementation of an adaptive finite-element approximation of the Mumford-Shah functional*, Numer. Math., 85 (2000), pp. 609–646.
[7] T. Brox, A. Bruhn, and J. Weickert, *Variational motion segmentation with level sets*, in Computer Vision – ECCV 2006, Lecture Notes in Comput. Sci. 3951, H. Bischof, A. Leonardis, and A. Pinz, eds., Springer, Berlin, 2006, pp. 471–483.
[8] A. Bruhn and J. Weickert, *A confidence measure for variational optic flow methods*, in Geometric Properties from Incomplete Data, R. Klette, R. Kozera, L. Noakes, and J. Weickert, eds., Springer, Dordrecht, The Netherlands, 2006, pp. 283–297.
[9] V. Caselles and B. Coll, *Snakes in movement*, SIAM J. Numer. Anal., 33 (1996), pp. 2445–2456.
[10] A. Chambolle and G. Dal Maso, *Discrete approximation of the Mumford-Shah functional in dimension two*, M2AN Math. Model. Numer. Anal., 33 (1999), pp. 651–672.
[11] Computer Vision Research Group, *Optical Flow Datasets*, University of Otago, New Zealand, 2005; http://www.cs.otago.ac.nz/research/vision.
[12] D. Cremers, T. Kohlberger, and C. Schnörr, *Nonlinear shape statistics in Mumford-Shah based segmentation*, in Proceedings of the 7th European Conference on Computer Vision, Copenhagen, Lecture Notes in Comput. Sci. 2351, A. Heyden, P. Johansen, M. Nielsen, and G. Sparr, eds., Springer, Berlin, 2002, pp. 93–108.
[13] D. Cremers and S. Soatto, *Motion competition: A variational approach to piecewise parametric motion segmentation*, Internat. J. Comput. Vision, 62 (2005), pp. 249–265.
[14] C. A. Davatzikos, R. N. Bryan, and J. L. Prince, *Image registration based on boundary mapping*, IEEE Trans. Medical Imaging, 15 (1996), pp. 112–115.
[15] M. Droske and W. Ring, *A Mumford–Shah level-set approach for geometric image registration*, SIAM J. Appl. Math., 66 (2006), pp. 2127–2148.
[16] M. Droske, W. Ring, and M. Rumpf, *Mumford-Shah based registration*, Comput. Vis. Sci., to appear.
[17] L. C. Evans and R. F. Gariepy, *Measure Theory and Fine Properties of Functions*, CRC Press, Boca Raton, FL, 1992.
[18] *Hamburg Taxi Sequence*, http://i21www.ira.uka.de/image_sequences.
[19] B. Horn and B. Schunk, *Determining optical flow*, Artificial Intelligence, 17 (1981), pp. 185–204.
[20] T. Kapur, L. Yezzi, and L. Zöllei, *A variational framework for joint segmentation and registration*, in the IEEE Workshop on Mathematical Methods in Biomedical Image Analysis (MMBIA 2001), IEEE Computer Society, 2001, pp. 44–51.
[21] S. L. Keeling and W. Ring, *Medical image registration and interpolation by optical flow with maximal rigidity*, J. Math. Imaging Vision, 23 (2005), pp. 47–65.
[22] P. Kornprobst, R. Deriche, and G. Aubert, *Image sequence analysis via partial differential equations*, J. Math. Imaging Vision, 11 (1999), pp. 5–26.
[23] E. Memin and P. Perez, *A multigrid approach for hierarchical motion estimation*, in Proceedings of the International Conference on Computer Vision (ICCV), 1998, pp. 933–938.
[24] D. Mumford and J. Shah, *Optimal approximation by piecewise smooth functions and associated variational problems*, Comm. Pure Appl. Math., 42 (1989), pp. 577–685.
[25] H.-H. Nagel and W. Enkelmann, *An investigation of smoothness constraints for the estimation of displacement vector fields from image sequences*, IEEE Trans. Pattern Anal. Mach. Intell., 8 (1986), pp. 565–593.
[26] P. Nesi, *Variational approach to optical flow estimation managing discontinuities*, Image Vision Comput., 11 (1993), pp. 419–439.
[27] J.-M. Odobez and P. Bouthemy, *Robust multiresolution estimation of parametric motion models*, J. Visual Commun. Image Representation, 6 (1995), pp. 348–365.
[28] J.-M. Odobez and P. Bouthemy, *Direct incremental model-based image motion segmentation for video analysis*, Signal Process., 66 (1998), pp. 143–155.
[29] N. Papenberg, A. Bruhn, T. Brox, S. Didas, and J. Weickert, *Highly accurate optic flow computation with theoretically justified warping*, Internat. J. Comput. Vision, 67 (2006), pp. 141–158.
[30] N. Paragios and R. Deriche, *Geodesic active contours and level sets for the detection and tracking of moving objects*, IEEE Trans. Pattern Anal. Mach. Intell., 22 (2000), pp. 266–280.
[31] O. Penrose and P. C. Fife, *Thermodynamically consistent models of phase-field type for the kinetics of phase transitions*, Phys. D, 43 (1990), pp. 44–62.

Copyright © by SIAM. Unauthorized reproduction of this article is prohibited.

[32] Y. Rathi, N. Vaswani, A. Tannenbaum, and A. Yezzi, *Particle filtering for geometric active contours with application to tracking moving and deforming objects*, in Proceedings of the 2005 IEEE Computer Society Conference on Computer Vision and Pattern Recognition (CVPR'05), Vol. 2, IEEE Computer Society, 2005, pp. 2–9.

[33] C. Schnörr, *Segmentation of visual motion by minimizing convex non-quadratic functionals*, in Proceedings of the 12th International Conference on Pattern Recognition, Jerusalem, Israel, 1994.

[34] M. Struwe, *Variational Methods: Applications to Nonlinear Partial Differential Equations and Hamiltonian Systems*, Springer, Berlin, 2000.

[35] G. Unal, G. Slabaugh, A. Yezzi, and J. Tyan, *Joint Segmentation and Non-Rigid Registration without Shape Priors*, Tech. report scr-04-tr-7495, Siemens Corporate Research, Princeton, NJ, 2004.

[36] B. Vemuri, J. Ye, Y. Chen, and C. Leonard, *Image registration via level-set motion: Applications to atlas-based segmentation*, Medical Image Anal., 7 (2003), pp. 1–20.

[37] J. Y. A. Wang and E. H. Adelson, *Representing moving images with layers*, IEEE Trans. Image Process., 3 (1994), pp. 625–638.

[38] S.-L. Wang, R. F. Sekerka, A. A. Wheeler, B. T. Murray, S. R. Coriell, R. J. Braun, and G. B. McFadden, *Thermodynamically-consistent phase-field models for solidification*, Phys. D, 69 (1993), pp. 189–200.

Copyright © by SIAM. Unauthorized reproduction of this article is prohibited.